inter.noise
21-24 AUGUST
SCOTTISH EVENT CAMPUS
GLASGOW 2022

Analysis and Control of Acoustic Modes in Cylindrical Cavities with application to Direct Field Acoustic Noise (DFAN) Testing

Jonathan A. Hargreaves[1]
Acoustics Research Group
Newton Building, University of Salford, Salford, M5 4WT, United Kingdom

ABSTRACT

It is well known that acoustic cavities have frequencies at which certain free-response 'modes' of propagation respond especially strongly. In the absence of significant damping, these cause peaks of high SPL in the frequency response as well as spatial non-uniformity and temporal ringing. The spatial non-uniformity is especially problematic since it means the room cannot be 'EQ'd' to compensate, since the SPL is different in different positions. This phenomenon has been studied extensively in the room acoustics literature and various strategies for mitigation proposed. Many of these make use of the theoretical mode shapes for a cuboid with a rigid boundary condition, since this is a common shape of room and a reasonable approximation for a solidly constructed wall. But modes exist for other shape spaces too. Of particular interest is the cylindrical cavity that is formed when large enclosing arrays of loudspeakers are used to perform high-intensity acoustic tests on space hardware. These possess problematic modes that can cause over-testing in some positions and under-testing in others. In this work, it is investigated how a simple FEM simulation can compute Q-factors for these modes and identify which will be problematic. How this might inform control system design is discussed.

1. INTRODUCTION

1.1 Modal Control in Room Acoustics

The acoustics of a room can affect quality of life for the people who live or work in it. A room modifies the sound a person hears, changing its frequency content and temporal structure [1]. This may cause musical notes to be emphasised or deemphasised and/or speech to become unintelligible. At high frequencies the dominant effect is reverberation, but at low frequencies 'room modes' are problematic. These can cause significant variation in SPL versus frequency and ringing artefacts, which have been shown to have an audible effect on reproduced music [2]. Often the focus has been on critical listening rooms, i.e., the control rooms where recorded music is mixed, since it is especially important that these are accurate and do not mask artefacts in recordings that would be audible in other rooms. But they can also affect environmental noise and its consequences [3].

Unsurprisingly, therefore, there is an extensive body of literature covering strategies to mitigate the effects of low frequency room modes. Historically, much of this has concerned room sizing and the application of passive absorbers [1], but electroacoustic solutions have also been suggested. Typically, this involves considering the placement of loudspeakers relative to the mode shapes of a room – these affect the positions from which modes are excited as well as where they are heard.

Welti and Devantier compared a variety of configurations and used a metric based on standard deviation of SPL to rank their performance [4]. This is a useful metric because SPL variation versus frequency can be EQ'd for (in principle), but SPL variation versus position cannot. For this reason, Pedersen recommended EQ'ing the room to flatten the average energy curve [5].

[1] j.a.hargreaves@salford.ac.uk

Celestinos and Nielsen [6] proposed arrays of subwoofers at opposite end of a cuboid room – each arranged to nullify lateral modes up to some given order – which are then driven with a delay designed to nullify end-to-end modes. Hargreaves and Wankling [7] implemented this scheme in a cuboid listening room, where it eliminated all modal effects below 75Hz and reduced the range of SPL variation (versus frequency and position) from around 25dB to within ±3dB post EQ'ing, a significant improvement. Recently, a method has been proposed based on a similar idea (nullifying the back wall reflection) but which attempts to do it adaptively for any incident sound field [8].

1.2 Direct Field Acoustic Noise (DFAN) Testing

Similar challenges present themselves in Direct Field Acoustic Noise (DFAN) Testing[2]. This is a technology developed for high-intensity acoustic testing, typically for qualification and pre-flight testing of satellite designs [9]. The launch environment, which typically lasts only a few minutes, is the most severe dynamic environment that a satellite will endure during its normal life. This testing aims to recreate the intense acoustic field the payload will be subjected to at launch in a controlled way in the laboratory, to verify a design can withstand this and so should complete its journey to orbit without damage. It has, therefore, become a mandatory part of the pre-flight testing process and is stipulated in launcher manuals for all payloads.

The most established way of conducting these tests is using a reverberation chamber. Like their counterparts in building acoustics, these have very low absorption and aim to subject the test article to a diffuse sound-field, a chaotic field in which acoustic waves arrive from every direction with equal power. This is chosen to ensure that any possible pattern of excitation which the test article might be especially sensitive to is included in the exciting sound field, i.e., it always includes the worst case. Testing for aerospace applications adds to this a requirement for Sound Pressure Levels (SPLs) that are enormously higher, usually requiring gas-powered electro-pneumatic noise sources mounted on giant horns. This, combined with the large size of the chambers, is a significant infrastructure investment. It also requires large delicate payloads to be transported to these facilities.

An alternative approach is to use electro-dynamic loudspeakers to generate the sound field. This approach has a history almost as long as reverberation chambers do, having been first suggested in 1966, and uses large arrays of adapted high-power concert sound loudspeakers. The approach is called DFAN, since the intention is that the 'Direct' sound field from the loudspeakers dominates over the reverberant sound from the enclosing room. This is achieved through proximity of the loudspeakers and use of a more typical room, which will have much higher absorption. A major advantage of this approach is portability – the test system can be brought to the test article.

Established best practice is to use a cylindrical array of loudspeakers encircling the test article. This subjects it to acoustic excitation from all angles – horizontally at least – while avoiding the risks associated with suspending heavy loudspeakers above a multi-million-dollar payload. The aim is to produce the same diffuse field that a reverberation chamber would, since this is the condition that standards, launches manuals and customers require. Arguably, DFAN is capable of much more than this – if every loudspeaker were controlled individually then it would implement Wave Field Synthesis [10] – and the launch environment inside a fairing has been shown to not be truly diffuse [11], but presently the demand is for diffuse fields and it is likely this will always be a requirement.

Problems arise, however, because the loudspeaker array is so big and so densely packed that it forms a cylindrical cavity that exhibits its own modes [12]. This is the same phenomena that compromises music reproduction in rooms, but the volume is now cylindrical instead of cuboid, giving the modes a different shape. Another key difference is that rooms are closed, so modal damping only occurs through losses due to absorbing materials in the room or wall compliance. In DFAN, the cavity is open at the top, so modal damping is largely due to radiation of energy out of this aperture or through the gaps between the loudspeaker stacks. Physical and practical limitations mean this configuration is unlikely to change, so interest lies in not exciting these modes in the first place, as is the aim of the methods for Room Acoustics proposed in refs. [4] and [6].

[2] DFAN Testing is also referred to in the literature and industry handbooks as DFAT (Direct Field Acoustic Testing). That acronym has been trademarked, however, so here the non-trademarked equivalent is used.

Research on how to best address issues with acoustics modes in DFAN has progressed down a very different path to the parallel work in Room Acoustics. Specifically, it has been informed by the state-of-the-art multi-axis shaker control [13]. Hence, there appears to be potential for bidirectional knowledge transfer. This paper aims at taking some first steps towards that aim.

1.3 Control and Forward Versus Adaptive 'Equalisation'

A key difference between how mode control is done in Room Acoustics and DFAN is whether these schemes can be regarded as forward 'equalisation' or adaptive 'control'. The difference is essentially whether the system is 'set and left', as is common in audio, or continually adjusted to meet a criterion. DFAN systems do the latter, typically with a Multi-Input Multi-Output (MIMO) controller, development of which is a research area in its own right [13–15].

Fundamentally this difference is due to what the two fields aim to achieve and how many 'drive' signals they use. Audio reproduction uses either a single drive signal (mono) or multiple drive signals (stereo or surround) that all contain different material and must each be considered separately. If a single monitor microphone position is used to check the reproduced SPL spectrum, as is commonplace, then the resulting equalisation process is single-input-single-output (SISO). Or if multiple microphones are monitored, as proposed by Pedersen [5], then this is multi-input-single-output (MISO). There is still only one 'drive' – the audio track to reproduce.

DFAN differs because there is no specific audio signal to be reproduced. Instead, there is just a target SPL curve that the produced noise needs to achieve, and this can be accomplished with multiple noise signals as drives. The 'random wave model' of diffuse fields [16] suggests that the number of drives should be maximized, and that these should be completely incoherent. But this would be very inefficient at low frequencies, since even a diffuse field shows some local coherence effect due to the long wavelengths [16]; driving speakers without considering this leads to substantial power loss due to destructive interference. A large drive count also incurs a severe computational overhead. Hence, DFAN typically uses a modest number of drives – 8 is a common choice – and the MIMO controller adapts the level of, and coherence between, noise signal drives to achieve a balance between uniformity of SPL and power efficiency.

DFAN control is, therefore, also adaptive. This lets it compensate, for example, for the reduction of loudspeaker efficiency during a test due to power compression. The controller monitors several microphones and adjust the drives to meet the target. This is a form of closed loop control, but what it implements is perhaps better termed *adaptive noise shaping*, because it is *noise shaping* that is *adapting* to (possibly changing) circumstances. Notably, the control loop is adapting very slowly compared to what would be required, for example, in Active Noise Control applications [17].

The consequence of this is that the MIMO controller will automatically eliminate modal effects, within the limits of: i) how well it can *observe* then, and ii) how well it can *control* them. These are important caveats that are termed *Controllability* and *Observability* in control system theory. These have a precise mathematical definition, but for the purposes herein the following definitions suffice:

- A system is controllable if there are enough drive channels (appropriately routed) that all possible aspects of the system's state can be controlled. In other words, no realisable system behaviour is beyond the influence of the controller.
- A system is observable if there are enough sensors (appropriately located) that all possible aspects of the system's state can be observed. In other words, no realisable system behaviour is unseen by the controller.

At low frequencies, the system's state is most readily expressed as the amplitudes (and phases) of all the modes. The modal summation equation, which is used to construct a system's Frequency Response (equivalently 'Room Transfer Function') from a summation of its modes [17], shows this. This is normally written for point sources and receivers, in which case the contribution of each mode depends on: i) the position of a source on the mode-shape, ii) the position of the receiver on the mode shape, and iii) the proximity of the driving frequency to the modes natural frequency and the mode's damping or decay rate. But for a large speaker array, as is used in DFAN, it is more appropriate to use a distributed model of boundary velocity in place of (i).

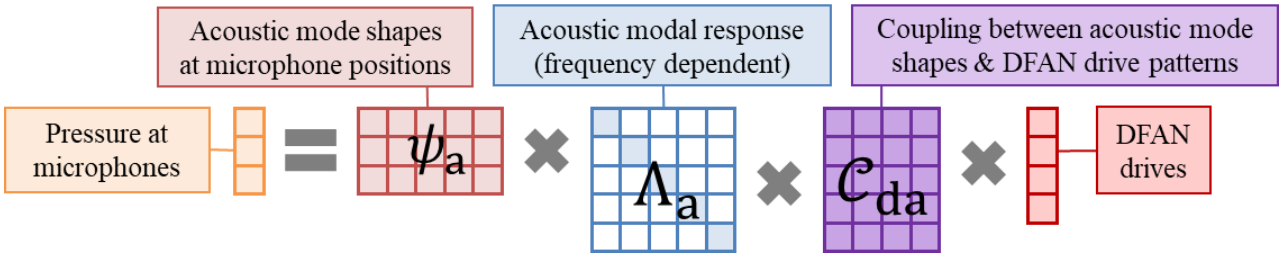

Figure 1: Modal summation model adapted to DFAN, showing 4 drives being transmitted to 3 microphones via 5 acoustic modes

Figure 1 shows the modal summation equation adapted to take this form. The pressure measured at each microphone is a vector of mode amplitudes (not shown) times a matrix of mode shapes $\boldsymbol{\psi}_a$. $\boldsymbol{\psi}_a$ is independent of drive frequency Each row in it corresponds to a microphone and each column to a mode – the entry where they cross is that mode shape evaluated at that microphone position.

The vector of mode amplitudes this responds to is found by the chain of terms on the right:

- The right most vector is the amplitudes of the DFAN drives output by the controller.
- $\boldsymbol{\Lambda}_a$ is a diagonal matrix that contains the frequency-dependent term for each mode. Its entries have magnitude inversely proportional to $|f_n^2 - f^2|$, where f_n is the (complex) eigenfrequency for this mode and f is the excitation frequency. It is diagonal because all modes operate independently.
- $\boldsymbol{\mathcal{C}}_{da}$ is a matrix that describes coupling between DFAN drives and acoustic modes. Each column corresponds to a drive signal and each row to an acoustic mode. Although the number of drives is finite, the acoustic source is now a continuous velocity distribution over a boundary – the faces of the loudspeaker cabinets. Entries in $\boldsymbol{\mathcal{C}}_{da}$ involve a boundary integral that computes the spatial match between the acoustic mode shape and the distribution of loudspeaker cones moving in response to a drive signal.

The ideal situation would be to have the controller able to observe and control all modes, but this is not possible because the number of modes grows rapidly with frequency and quickly exceeds the number of microphones and drives. Substantially increasing the number of these to mitigate this is not feasible because it adds significant computational cost to the control algorithm, meaning compromises would have to be made in frequency resolution and/or control loop update rate.

A better strategy is therefore required. It is well known in Room Acoustics that some modes are more troublesome than others. This is usually to do with their damping, or inversely, their Q-factor. This has been witnessed in DFAN too. Kolaini *et al.* [12] showed that problem frequencies correlate with modes, but did not emphasise the large proportion of modes that are *not* problematic. The question is therefore how to identify which modes are problematic and which ones aren't, so it can be ensured that the controller can control and observe the problematic ones.

Figure 1 shows that $\boldsymbol{\psi}_a$ and $\boldsymbol{\mathcal{C}}_{da}$ respectively describe the observability and controllability of modes. These are, therefore, respectively defined by microphone positions and loudspeaker drive distributions. Altering the position of control microphones to optimize observability has previously been explored [18], but designing drive distributions to optimize controllability has not. MSI-DFAT call this their "Drive Matrix Switch" but, while there has been some discussion of it in the literature [19], its effect on modal coupling does not appear to have been considered

The premise explored in this paper, therefore, is how the drive channels of the controller might be routed so that they optimally control modes that are identified as being the most problematic.

1.4 Contribution by this paper

This paper develops a methodology for optimizing the DFAN drive signal to loudspeaker routing matrix that is informed by a modal analysis. This idea has similarities to Wave-Domain Adaptive Filtering [10], in which families of solutions of the acoustic wave equation are used to map between drive channels and loudspeakers. The difference here is that the mapping is informed by modes of the physical space in question (albeit idealised), as are used for Room Acoustic equalisation in refs.

[4] and [6]. Compared to those, the difference is that they aimed to completely avoid excitation of those modes through spatial drive patterns that are applied to all frequencies. Here, the aim is rather the opposite, due to the use of the MIMO controller. It is to make drive patterns associated with problem modes available to the controller, so it can utilise them away from problem frequencies and attenuate them when needed. Hence, we aim to match drive patterns with problem modes.

Section 2 presents an analytical model of modes in a DFAN cavity following Kolaini *et al.* [12]. Section 3 presents a similar but slightly more realistic FEM model. This remains extremely simple but is able to calculate Q-factors for modes, and thereby rank how problematic they are likely to be. Section 4 uses this information to design a DFAN drive map and utilise it in a simulated MIMO controller. Finally, section 5 draws conclusions and lists some avenues for future research.

2. ANALYTICAL MODEL OF MODES IN A DFAN CAVITY

The Finite Element Method (FEM) can solve for eigenmodes of a cavity of arbitrary shape. It also has the capability to include absorption mechanism that damp the mode and find its Q-factor. These advantages will be exploited in section 4. But analytical models of modes remain extremely informative for geometries where they exist. Notably, they can be indexed in meaningful ways and usually take simple mathematical forms that provide an engineer with useful insight.

In this section an analytical model of modes in a DFAN cavity will be presented. This follows ref. [12] but is included here because the presentation there is incomplete. Notably, the separated partial differential equation and boundary conditions are stated, but the final form of the solution is not. Additionally, the results are not presented in an especially clear way and do not appear to agree with our calculations, which have been validated using a commercial FEM code.

The model is defined in cylindrical coordinates; radius r, azimuth θ and height z. Its dimensions match the cylinder used in ref. [12], which is based on the 2011 tests at Johns Hopkins University Applied Physics Laboratory (APL), as also reported by Maahs [20,21]. It has height $Z = 150" \approx 3.81\text{m}$ and radius $R = 96" \approx 2.4\text{m}$. The boundary conditions applied in the model were as follows:

- Rigid floor: $\partial P/\partial z = 0$ at $z = 0$.
- Rigid loudspeaker stacks: $\partial P/\partial r = 0$ at $r = R$.
- Top of stack pressure release condition: $P(Z) = 0$.

Since this is a 3D problem, there are three mode indices. These are azimuthal mode number m, radial mode number n and vertical mode number l. The mode shapes have the form:

$$\psi_{m.n.l}(r,\theta,z) = J_m\left(k_{m,n}r\right) \times \cos(k_l z) \times \begin{cases}\cos(m\theta)\\ \sin(m\theta)\end{cases}. \tag{1}$$

Here J_m is a Bessel function of order m, $k_{m,n}$ is the wavenumber component in the horizontal plane, and k_l is the wavenumber in the vertical plane. Variants with sine and cosine dependence are required to form a complete basis, but they are identical except for a $90°/m$ rotational shift.

Examples of these mode shapes are shown in Figure 2. It can be observed that these all tend to zero as $z \to Z$ to satisfy the $P(Z) = 0$ boundary condition. To achieve this, valid values of k_l are

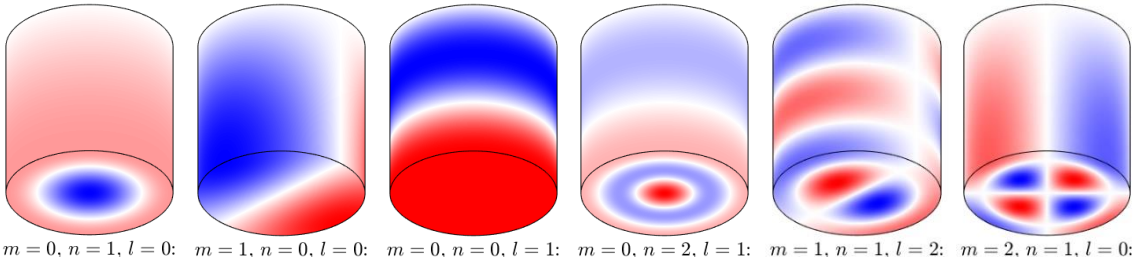

Figure 2: Examples of analytical mode shapes for various values of m, n and l. Red, blue, and white respectively indicate in-phase, anti-phase, and zero pressure.

This document is slightly extended compared to the published version. It includes some additional equations and explanation that had to be cut to fit into the page count prescribed by the proceedings, but which are reinstated here.

$k_l = 2\pi(2l+1)/4Z$. Valid values of $k_{m,n}$ correspond to the n^{th} value of kr for which $dJ_m/dr\,(kr) = 0$ at $r = R$. More commonly, one would convert to normalised radial wavenumber $\kappa_{m,n} = k_{m,n}R$ and then search for the n^{th} value of κ for which $dJ_m/d\kappa\,(\kappa) = 0$. These points can be computed by a search routine or looked in up tables, e.g., eq. 6.28 in [22].

The total wavenumber $k_{m,n,l}$ of a given mode is found by $k_{m,n,l}^2 = k_{m,n}^2 + k_l^2$, and its frequency can be found by $f_{m,n,l} = k_{m,n,l} \times c_0/2\pi$, where $c_0 = 343\text{ms}^{-1}$ is the speed of sound in air. Natural mode frequencies $f_{m,n,l}$ predicted by this are given in column 3 of Table 1, there titled "$f_{p=0}$" to acknowledge the boundary condition used at $z = Z$. A peculiarity is that none of these match the frequencies given in ref [12], the reason for which is not known. The frequencies presented in this report have been validated against a commercial FEM package simulating the same problem.

2.1 Discussion of the realism of the analytical model for DFAN applications

The analytical model above solves the Helmholtz equation for an idealised version of a DFAN cavity. Notably, real cavities are not truly cylindrical. They are made up of stacks of speakers with flat faces, with gaps in-between, and some (usually subwoofers) may be set back slightly. The boundary conditions are also approximate. Here, their realism should be considered.

The rigid floor condition is a realistic assumption. Test chambers have floors of extremely heavy construction. The loudspeaker stack rigid boundary condition is also fairly realistic. Factors it omits includes the gaps between the loudspeakers and the compliance of the loudspeaker drivers. The former is quite small, however, so can either be ignored or could be accounted for by an appropriate slit impedance [1]. The latter could be accounted for with an impedance boundary condition.

The boundary condition at top of the cavity includes the most approximation. In reality there is no boundary here; the loudspeaker array stops but the air continues. An analytical model requires a boundary condition to be chosen, however. The pressure release condition chosen by Kolaini *et al* is a reasonable first approximation but is not realistic and overestimates resonant frequencies. For equivalent pipe resonance or duct radiation problems, it is common to use an 'end correction' [23]. This adds some hypothetical extra length onto the end of the pipe to account for the additional mass of air that is not inside the pipe, but which moves with it. Such an approach could be used here, but standard corrections only exist for the zeroth radial and azimuthal mode orders.

Another issue is that none of the boundary conditions allow energy to escape, hence modes do not decay and their Q-factors cannot be calculated. Inclusion of boundary impedances and radiation loss through the top aperture would allow Q-factor to be found, but this would complicate the model substantially. Hence it is easier to resort to numerical methods, as is done in the next section.

3. FINITE ELEMENT METHOD (FEM) MODEL OF MODES IN A DFAN CAVITY

As discussed above, the biggest source of approximation in the analytical model is the inability for acoustic energy to escape through the aperture at the top of the cavity. The FEM model reported in this section was conceived to investigate that limitation, hence all other aspects are identical.

The geometry remains axisymmetric, like the analytical model. A radial slice is shown in Figure 3a and the 3D geometry arising from its rotation (minus a 120° cut-out) is shown in Figure 3b. The grey area is the acoustic domain, and the blue regions are Perfectly Matched Layers (PMLs). These are used to terminate the mesh without reflection, meaning the model is performed as if it were an in an unbounded half-space above a rigid ground plane. The vertical gap in the air domain is where the loudspeaker stacks are located. The inner radius and height of the array are 2.4m and 3.81m respectively, matching the 2011 tests at APL and the analytical model, and individual loudspeaker stacks and the gaps between them are still not modelled. The thickness of this is chosen to be 0.5m, a typical depth for line array loudspeakers. The air behind the stack was included in the model because the geometry surrounding an aperture is known to affect end-correction formulae [23].

Two studies were conducted. The study that finds the mode shapes and frequencies is called an eigenfrequency study. For this, all boundaries are rigid. The second study computes the frequency response of the system to time-harmonic excitation. This comes from the loudspeakers, so a normal velocity boundary condition is applied to their inward face (coloured green in Figure 3a).

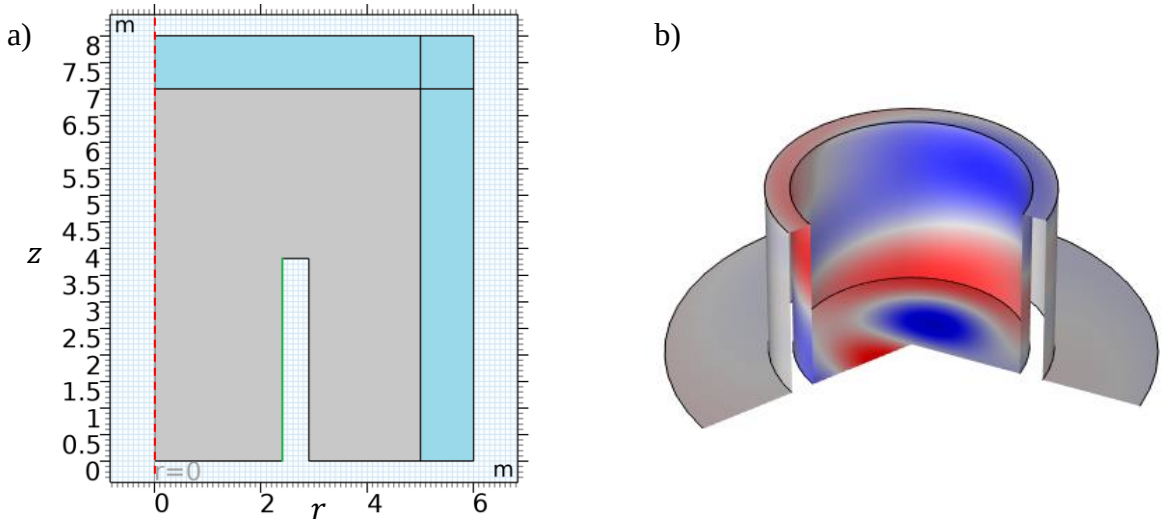

Figure 3: a) Radial slice through the geometry modelled in FEM. The blue region is a PML, the green line is the velocity boundary condition, and the red dashed line is the axis of symmetry. b) 240° slice from the revolved geometry including the real part of a boundary pressure field.

Use of axisymmetry also significantly expedites numerical solution of the problem in FEM. It allows the Partial Differential Equation (PDE) being solved using FEM to be simplified, such that only the 2D slice shown in Figure 3a need be meshed and solved for. The full 3D solution $\psi^{3\mathrm{D}}_{m.n.l}(r,\theta,z)$ is found from the 2D solution $\psi^{2\mathrm{D}}_{m.n.l}(r,z)$ – which FEM computes – by:

$$\psi^{3\mathrm{D}}_{m.n.l}(r,\theta,z) = \psi^{2\mathrm{D}}_{m.n.l}(r,z) \times \begin{cases} \cos(m\theta) \\ \sin(m\theta) \end{cases}. \tag{2}$$

This has the same form as eq. 1, but FEM is computing $\psi^{2\mathrm{D}}_{m.n.l}(r,z)$ numerically instead of it being stated analytical as the product of a Bessel and a cosine function. Azimuthal mode number m is an argument passed to the FEM solver, so solutions can still be calculated for a range of values of m. $0 \leq m \leq 4$ was used for the eigenfrequency study and $0 \leq m \leq 3$ for the frequency response.

The simulations were performed in COMSOL Multiphysics v5.4 using a mesh of 936 quadratic Lagrange quadrilateral elements smaller than 0.23m. This is roughly $\lambda/5$ at the highest frequency simulated (300Hz). The PML was of the 'rational' type with both scaling factors set to 2.

3.1 Eigenfrequency Study Results

While this geometry remains simple, the aperture at the top of the cavity allows it to radiate energy, hence its modes are damped in a realistic way. This can be quantified from the frequency response via Q-factor, the ratio of peak centre-frequency to half-power bandwidth. Another useful metric is Modal Decay Time MT_{60}, the time in seconds it takes a mode to decay by 60dB. Both of these can be found from the FEM eigenfrequencies, which are complex for a damped problem [24]. Q-factor is equal to $\mathrm{real}(f_{n,m,l})/2 \times \mathrm{imag}(f_{n,m,l})$ and $MT_{60,n,m.l} = 3\ln(10)/2\pi \times \mathrm{imag}(f_{n,m,l})$.

Table 1 presents these metrics for the FEM model, along with its eigenfrequencies and those of the analytical model. A colour scale is used to emphasise high values. Care has been taken to match the modes between the FEM and analytical model, which is necessary because a FEM solver does not index them in n or l – it just returns them in ascending order of frequency. This matching process is non-trivial since modes from the two models are not identical, and the FEM solver finds many extra highly damped modes that are of little physical importance. Modes were matched using the Modal Assurance Criterion [24] and similarity of eigenfrequency. Matches are typically clear cut for important high-Q modes but may be ambiguous or not possible for highly damped modes.

m	n	l	$f_{p=0}$ (Hz)	f_{FEM} (Hz)	Q-factor	MT_{60} (s)
0	0	0	22.51	16.35	8.28	1.11
1	0	0	47.54	45.49	45.28	2.19
0	0	1	67.52	51.41	2.99	0.13
2	0	0	73.03	71.91	133.65	4.09
1	0	1	79.45	67.77	6.93	0.22
0	1	0	90.01	89.10	91.01	2.25
2	0	1	96.88	89.46	13.02	0.32
3	0	0	98.17	97.45	221.98	5.01
0	1	1	110.25	103.06	14.59	0.31
0	0	2	112.54	-	-	-
3	0	1	117.01	111.56	24.74	0.49
1	0	2	120.08	114.83	2.98	0.06
4	0	0	123.03	122.51	372.55	6.69
1	1	0	123.34	122.68	181.28	3.25
2	0	2	132.25	120.16	4.95	0.09
4	0	1	138.52	134.43	36.00	0.59
1	1	1	138.80	134.13	19.49	0.32
0	1	2	142.34	131.50	5.53	0.09
3	0	2	147.63	137.56	9.38	0.15
2	1	0	154.19	153.78	275.89	3.94
0	0	3	157.56	-	-	-
0	2	0	161.16	160.76	288.11	3.94
1	0	3	163.03	-	-	-
4	0	2	165.21	156.58	13.84	0.19
1	1	2	165.44	155.59	9.32	0.13
2	1	1	166.82	163.47	36.66	0.49
2	0	3	172.19	159.46	4.57	0.06
0	2	1	173.28	170.09	36.14	0.47
0	1	3	180.06	-	-	-
3	1	0	183.70	183.36	469.68	5.63
3	0	3	184.27	171.99	6.37	0.08
2	1	2	189.56	181.55	12.17	0.15
3	1	1	194.42	191.56	45.97	0.53
0	2	2	195.27	187.72	13.34	0.16
1	2	0	195.49	195.20	512.52	5.77
4	0	3	198.63	187.29	8.83	0.10
1	1	3	198.82	187.61	5.38	0.06

Table 1: Comparison of natural frequencies from the analytical model of the APL test cavity versus those computed with axisymmetric FEM, for $f < 200$Hz and $m \leq 4$. Q-factor and Modal Decay Time MT_{60} are for the FEM result. The colour scale emphasises high values of Q and MT_{60}.

Q-factor and MT_{60} both quantify energy trapping. Large values indicate problem modes with trapped energy, while small values indicate fast decay due to rapid energy loss. Q-factor is the more established metric, but the data in Table 1 shows that MT_{60} occupies a more consistent range.

What is evident from both metrics is that the degree of energy trapping varies significantly between modes, and that modes with $l = 0$ trap energy the most. This makes sense because modes also have a ray-orbit interpretation: modes with $m \neq 0$ are spinning around the cavity; modes with $n \neq 0$ are contracting and re-expanding radially; and modes with $l \neq 0$ are travelling up and down.

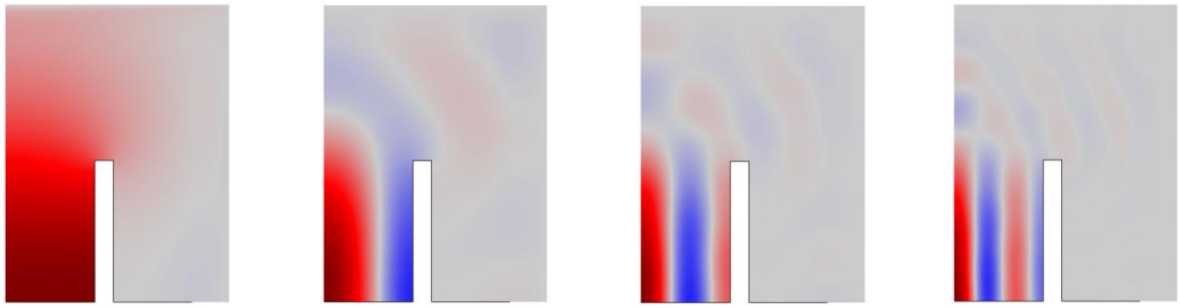

[0 0 0]	[0 1 0]	[0 2 0]	[0 3 0]
16.35Hz	89.09Hz	160.76Hz	232.35Hz
Q = 8.28	Q = 91.01	Q = 288.11	Q = 657.95
MT_{60} = 1.11s	MT_{60} = 2.25s	MT_{60} = 3.94s	MT_{60} = 6.23s

Figure 4: Radial cross-sections through FEM mode shapes with $m = l = 0$, for four values of n

Since energy loss occurs at the top of the cavity, it follows that those modes with $l \neq 0$ interact with this aperture most often and therefore experience the fastest rate of energy loss.

Figure 4 illustrates how different mode shapes can be trapped to different extents, and how there affects their Q-factor and MT_{60}. The zeroth mode, with $m = n = l = 0$, is a wave that escapes into the surrounding enviroment. But this effect reduces as l increases, and by $l = 3$ there is a very high-Q radial standing wave present that is trapped and experiences little energy loss to radiation.

3.2 Frequency Response Results

Figure 5 shows frequency results arising from the same model for $m \leq 3$. The response for each value of m is shown separately. This is justified because the modes and driving functions are perfectly orthogonal in azimuthal angle due to the perfect axisymmetry.

As expected, the peaks align perfectly with the high-Q eigenfrequencies, which all occur for $l = 0$. Some other transitory damped peaks appear, e.g., the [3 0 1] mode marked at 111.5Hz, but the majority are sufficiently damped so as to be indistinguishable. This result validates one premise of the paper, that high-Q modes are worth searching for since it is these that cause SPL peaks.

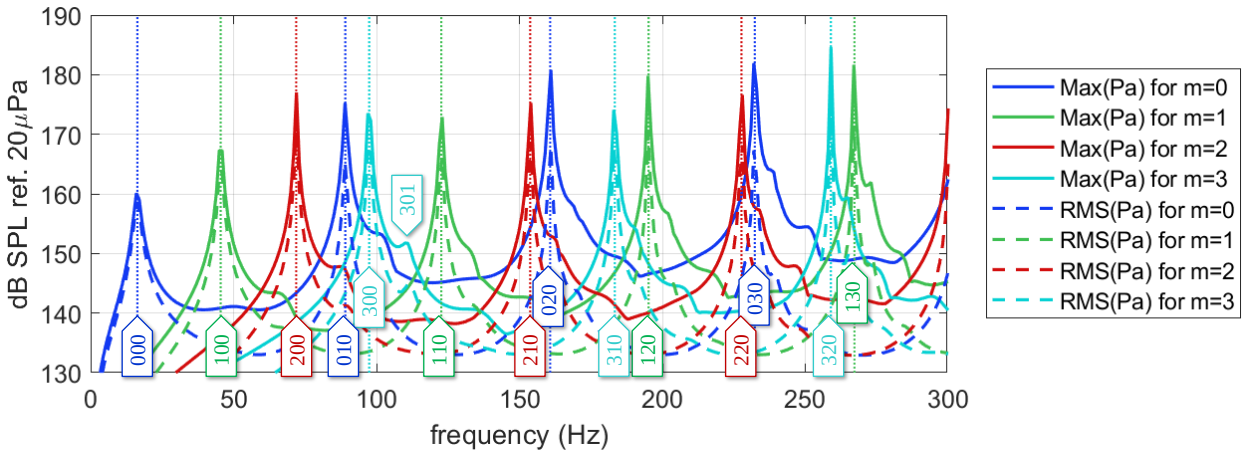

Figure 5: Spatially averaged frequency response for 1mm/s vibration of the loudspeaker array surface. Solid lines are maximum pressure in the cavity. Dashed lines are RMS pressure. Both are plotted as dB SPL. Results are shown separately for different values of azimuthal mode number m, and high-Q eigenfrequencies are overlayed (vertical dotted lines and mnl markers).

3.3 Comparison with the measurements reported by Kolaini *et al.* (2012)

Modes with $l = 0$ were also the most likely to have been excited by the DFAN configurations tested at APL in 2011. Maahs [21] reported that several drive configurations were investigated. In the MISO case, all the loudspeakers were fed by the same drive. This will mainly excite modes with

$m = 0$ and $l = 0$. For the MIMO case, there were 12 independent drives each feeding a loudspeaker stack. This will excite modes with a variety of values of m, but still only with $l = 0$.

Kolaini *et al.* analysed data from these same tests. Figure 3 in ref. [12] presents the SPL results. In the MISO case, problem frequencies were identified as being 93 Hz and 229 Hz, which match well with the 89.1 Hz [0 1 0] Q = 91.01 mode in Table 1 and the 233.6 Hz [0 3 0] Q = 657.9 mode (not included in Table 1 but shown in Figure 5). These modes have $m = 0$, as expected when all loudspeaker stacks are fed the same signal; the drive pattern is $m = 0$ too. Notably the 97.45Hz [3 0 0] and 122.5Hz [4 0 0] modes are both high-Q but are not excited since they have $m \neq 0$.

The MIMO drive caused a different response, despite the modes of the acoustic system being unchanged, because they are excited differently by the different drive pattern. Kolaini *et al.* report that the lower frequency problem mode increases in frequency to 95Hz, but it is more likely that this is the combination of two modes: [0 1 0] (89.1 Hz), as originally excited, plus [3 0 0] mode (97.45Hz), which is now excited due to the circumferential decorrelation in the excitation field. The right-hand plot of fig. 3 in ref. [12] also shows far more modes being excited (note the vertical axis is PSD on a linear scale, which makes them look small relative to the peaks – they would look more significant on a dB scale). This now appears to also include the [0 2 0] mode (160.7Hz) that Table 1 predicts should be significant, but which doesn't appear to be in the MISO case.

In summary, Kolaini *et al. explained* the measured behaviour using the modes of the analytical model. That is a useful contribution, but it neglects to mention the large number of other modes that are not excited and proposes no methodology for predicting which ones are problematic. This study has addressed that need with a simple FEM model for which Q-factor can be computed.

4. APPLICATION TO DFAN DRIVE MAP DESIGN

The results above show that drive patterns can affect the excitation of modes. In single-drive Room Acoustics applications, the objective would be to design a drive pattern that would not excite those modes. But in DFAN the presence of the MIMO controller turns this logic on its head. Instead, it is beneficial to include drive patterns that match with problem modes, so the controller has control of them. This section aims to demonstrate that mechanism.

The most problematic modes all have $l = 0$. Matching this with drives amounts to driving all loudspeakers in each column with the same signal, as is likely to be common practice. The DFAN literature does not generally report this signal routing, but wiring columns together is easiest and is standard practice in concert sound, and in various photographs it appears that this is what was done.

16 control and 8 monitor mics were simulated. The positions of these were chosen randomly with radius $0 \leq r \leq 1.5\text{m}$ and heigh $0.5\text{m} \leq z \leq 2.5\text{m}$, to ensure they were more than 0.9m from the loudspeakers and not too close to the floor, following best practice recommended in NASA-HDBK-7010. Seven drive patterns were used: uniform, $\cos(\theta)$, $\sin(\theta)$, $\cos(2\theta)$, $\sin(2\theta)$, $\cos(3\theta)$, and $\sin(3\theta)$. In a axisymmetric FEM model this is easier to implement than driving each angle sector (representing a loudspeaker stack) separately, but it is approximately a linear recombination of those patterns, so is roughly equivalent. Pressure at the microphones was computed using eq. 2.

Transfer functions from drives to microphones were exported from COMSOL and postprocessed in Matlab. At each frequency, this yields a matrix $\mathbf{H}$ that relates drive amplitudes to pressure at the microphones $\mathbf{p}$ by $\mathbf{p} = \mathbf{H}\mathbf{d}$. DFAN control is, however, done in terms of power statistics [13,15]. This involves squaring $\mathbf{d}$ and $\mathbf{p}$, which in matrix notation is $\mathbf{S}_{\text{dd}} = \langle \mathbf{d}\mathbf{d}^H \rangle$ and $\mathbf{S}_{\text{pp}} = \langle \mathbf{p}\mathbf{p}^H \rangle$. Here, superscript H denotes Hermitian (conjugate) transpose and angled brackets $\langle \cdots \rangle$ denote averaging over multiple FFT periods, as is a standard part of FFT-based transfer function measurement. $\mathbf{S}_{\text{dd}}$ and $\mathbf{S}_{\text{pp}}$ are the Spectral Density Matrices (SDMs) for the drive and the microphone signals respectively. These are square and their diagonal gives the power in each signal. The off-diagonals are the square root of the product of the powers of a pair of signals, multiplied by their coherence and a phase term [15]. Hence, the diagonal of $\mathbf{S}_{\text{pp}}$ can be used to find the SPL at the microphones.

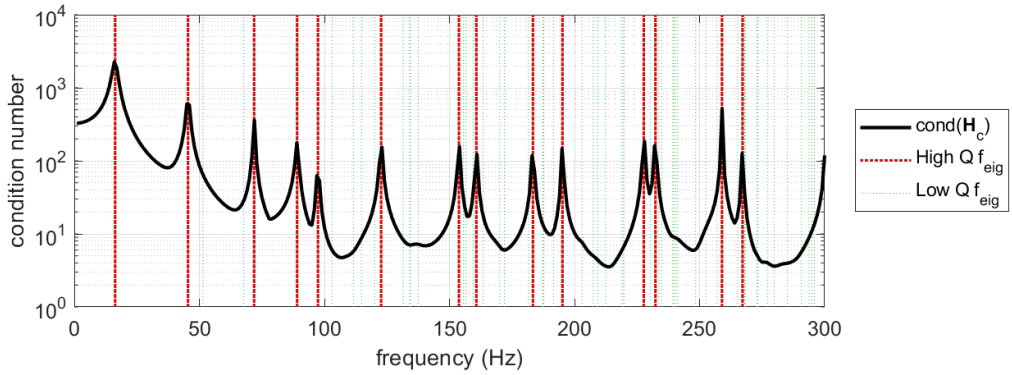

Figure 6: Condition number trends for the drive to control mic transfer function matrix $\mathbf{H}_c$. Mode frequencies with high Q are highlighted in red and those with lower Q in green.

Control is achieved by specifying a target SDM $\mathbf{S}_{tt}$ that should be achieved at the control microphones. This encapsulates the SPL and coherence requirements. The optimal drive SDM $\mathbf{S}_{dd}$ (off-diagonals of which are complex, so include relative phase) can be found by [15]:

$$\mathbf{S}_{dd} = \mathbf{H}_c^{\dagger}\mathbf{S}_{tt}\left(\mathbf{H}_c^{\dagger}\right)^{H}. \tag{3}$$

Here $\mathbf{H}_c$ is the row-wise subset of $\mathbf{H}$ pertaining to the control microphones. The dagger symbol † indicates a Moore-Penrose pseudo-inverse. The latter is required because rectangular MIMO uses more control microphones than drives. This means that $\mathbf{S}_{pp}$ will not exactly equal $\mathbf{S}_{tt}$ at all the control microphones, but it has the benefit of forcing the controller to concentrate on readily realizable behavior that translates to all locations, including the monitor mics [14,15]. In contrast, square control – which uses the same number of control mics as drives – tends to use excessive drive power to chase precision at the control mic locations at the expense of deviations elsewhere.

Finally, the SPL responses at all microphones are found from the diagonal of $\mathbf{S}_{pp}$ computed by:

$$\mathbf{S}_{pp} = \mathbf{H}\mathbf{S}_{dd}\mathbf{H}^{H}. \tag{4}$$

4.1 Results

The compromise present in the pseudo-inversion is quantified by the condition number of $\mathbf{H}_c$, being the ratio of its smallest and largest singular values. This is presented in Figure 6 above. It can be seen that condition number peaks at frequencies of high Q modes (shown in red), indicating that a single behaviour (the mode) is present in the matrix that dominates all others. Lower Q modes found by the eigenfrequency solver, shown in green, do not have this drastic effect.

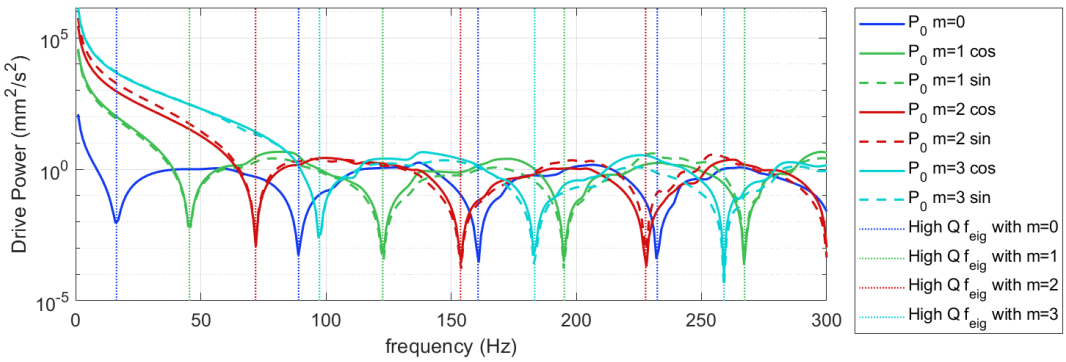

Figure 7: Drive power versus frequency. Mode frequencies with high Q are highlighted with vertical lines. Colour indicates azimuthal mode number.

This document is slightly extended compared to the published version. It includes some additional equations and explanation that had to be cut to fit into the page count prescribed by the proceedings, but which are reinstated here.

Figure 7 shows the drive power that the controller sends to the loudspeakers. Since these were represented by a velocity boundary condition in the FEM model, the units of this is mm^2/s^2. It can be seen that the controller 'turns down' the drives that would excite problem modes at the frequencies where they occur, but utilises them at other frequencies to transmit power and improve homogeneity. The result is that Figure 7 is rather like an upside-down version of Figure 5. The high drive amplitudes at low frequencies arise to compensate for the low radiation efficiency of the velocity boundary condition at low frequencies, and a minima that occurs at $kr \approx 0$ for modes with $m > 0$. In reality, subwoofers use ports and horns to produce high volume velocity, so have a frequency response that would counteract this effect. Overly high drive powers can be inhibited by introducing their norm into the matrix pseudo-inversion, as is done by Tikonov regularisation.

Figure 7 is an idealised version of what would happen in a real system. The axisymmetry has given the modes and driving functions perfect orthogonality, meaning each m acts independently. In a real system one would expect similar behaviour but with more interaction due to the absence of orthogonality. Note that both cosine and sine drives were required to achieve full control. Omitting one or other caused significant deviations in some monitor mic SPLs at some frequencies.

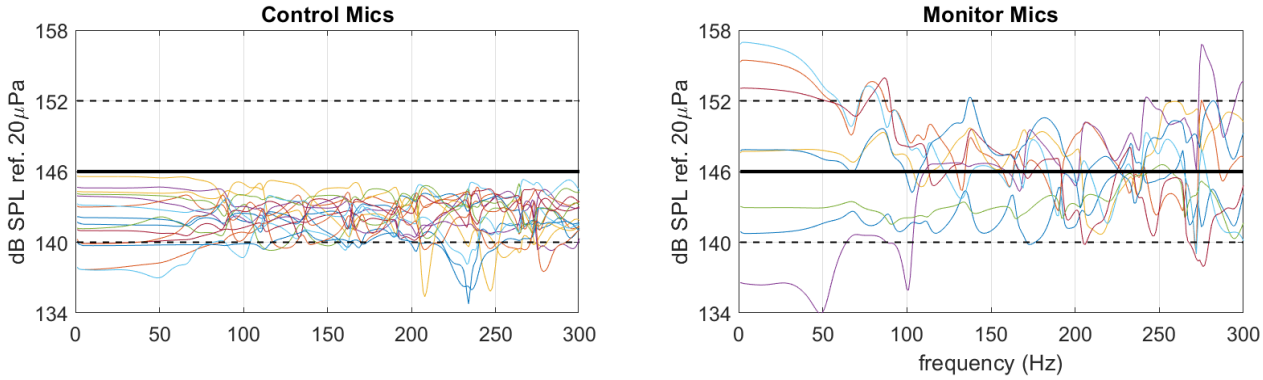

Figure 8: SPL responses at the control mics (left) and monitor mics (right) versus frequency

Figure 8 shows the SPL at the control and monitor mics. $\mathbf{S}_{tt}$ was set so as to give a target SPL of 146dB at all mics, indicated by the thick black line. It can be seen that in both cases SPLs are close to the target, though not as close as is achieved by state-of-the-art controllers. Herein, $\mathbf{S}_{tt}$ was set following the diffuse field $\mathrm{sinc}^2\, kR$ theoretical coherence trend [16], but recent research has studied how this might be done optimally [14]. Notably, the control mics mostly have a tight standard deviation, but their mean sits a few dB below the target, whereas the monitor mic SPLs are more spread but have the correct mean. This phenomenon has been reported elsewhere in the literature. Alvarez Blanco *et al* refer to it as the "Energy sink" [15]. Experiments here showed that increasing the number of control microphones increased this effect but tightened the monitor mic spread.

5. CONCLUSIONS

This study has considered how modal analysis might inform DFAN drive patterns. These are not often reported in the DFAN literature, but this work shows that they should be since they have a significant effect on mode control. A FEM model of a simplified cylindrical DFAN cavity was created for this purpose. This is only slightly more detailed than the accepted analytical model but has the important advantage that it can predict Q-factors and modal decay times, which can be used to rank which modes are likely to be problematic. These were seen to tally very well with the measurements of the 2011 APL tests published by Kolaini *et al.* in 2012. Notably, the methodology herein *predicts* which modes will be problematic, whereas prior work only aims to *explain* them.

Design of drive patterns to allow control of problematic modes was then considered. This led to patterns equivalent to loudspeakers being driven in stacks, as is believed to be common practice. Transfer functions from the model were then inserted into a MIMO control system model, allowing the response of the control algorithm to modes of different orders to be observed.

This document is slightly extended compared to the published version. It includes some additional equations and explanation that had to be cut to fit into the page count prescribed by the proceedings, but which are reinstated here.

5.1 Avenues for Future Research

This was not a high-fidelity model of a DFAN test so is extremely idealised. It does not even include a payload, which fig. 14 of NASA-HDBK-7010 shows has a significant effect. But it has the significant benefit over more detailed models of being very simple, while also providing useful information that the analytical model cannot. Hence, it appears to be a quick yet useful approach. But nonetheless, a study to explore whether these findings extend to a more realistic configuration should be conducted. Some models of DFAN have been very sophisticated [25].

Since the acoustic domain is unbounded a BEM solver might be advantageous. Historically these have only been able to compute frequency response results but eigenfrequency solvers for BEM are emerging [24]. This would avoid the need to choose PML parameters, which were found to affect the Q-factor of the lowest frequency modes.

Other drives with $l \neq 0$ should also be tested to see how they perform. A configuration using $l = 1$ drive patterns was briefly investigated and showed little improvement. But this was not done thoroughly and should be investigated further.

Different target SDMs could also be investigated. Recently the phase of off-diagonal terms has been manipulated to render a directional wave [26], emphasising the parallels between DFAN and Wave Field Synthesis [27]. MIMO control theory could also be applied to mode control in Room Acoustics; rather than manually design a loudspeaker layout to nullify modal excitation, regularised matrix inversion could be used to find frequency-dependent drive patterns that minimise this.

Finally, metrics for sound field diffuseness should also be added to the study. Coherence between different microphone positions is most widely used in practice [28], but measures based on intensity and isotropy [29] are also possible.

ACKNOWLEDGEMENTS

The novel contributions reported in this paper received no external funding, but the work draws heavily on a literature review [9] that was commissioned and funded by RAL Space (STFC).

REFERENCES

[1] T.J. Cox, P. D'Antonio, Acoustic Absorbers and Diffusers: Theory, Design and Application, 2nd ed., Taylor & Francis, 2009.

[2] B.M. Fazenda, M. Stephenson, A. Goldberg, Perceptual thresholds for the effects of room modes as a function of modal decay, J. Acoust. Soc. Am. 137 (2015) 1088–1098. https://doi.org/10.1121/1.4908217.

[3] A.T. Moorhouse, D.C. Waddington, M.D. Adams, A procedure for the assessment of low frequency noise complaints, J. Acoust. Soc. Am. 126 (2009) 1131–1141. https://doi.org/10.1121/1.3180695.

[4] T. Welti, A. Devantier, Low-Frequency Optimization Using Multiple Subwoofers, J. Audio Eng. Soc. 54 (2006) 347–364.

[5] J.A. Pedersen, Convention Paper 7261 Sampling the Energy in a 3D Sound Field, in: Proc. Audio Eng. Soc., New York, 2007.

[6] A. Celestinos, S.B. Nielsen, Controlled Acoustic Bass System (CABS) A Method to Achieve Uniform Sound Field Distribution at Low Frequencies in Rectangular Rooms, J. Audio Eng. Soc. 56 (2008) 915–931.

[7] J.A. Hargreaves, M. Wankling, Implementing wave field synthesis in an ITU spec listening room part 2: Bass without modes, in: Proc. Inst. Acoust., Brighton, 2011.

[8] F.M. Heuchel, E. Fernandez-Grande, F.T. Agerkvist, E. Shabalina, Active room compensation for sound reinforcement using sound field separation techniques, J. Acoust. Soc. Am. 143 (2018) 1346–1354. https://doi.org/10.1121/1.5024903.

[9] J.A. Hargreaves, Literature review of Direct Field Acoustic Noise (DFAN) testing, Salford, 2022. https://doi.org/10.17866/h20g-8587.

[10] S. Spors, H. Buchner, R. Rabenstein, W. Herbordt, Active listening room compensation for

massive multichannel sound reproduction systems using wave-domain adaptive filtering, J. Acoust. Soc. Am. 122 (2007) 354–369. https://doi.org/10.1121/1.2737669.
[11] B. Gardner, Observations of the Sound Field During Liftoff of the Cassini Spacecraft, in: Proc. Spacecr. Launch Veh. Dyn. Environ. Work., 2000.
[12] A.R. Kolaini, B. Doty, Z. Chang, Impact of Acoustic Standing Waves on Structural Responses: Reverberant Acoustic Testing (RAT) vs. Direct Field Acoustic Testing (DFAT), in: Proc. 28th Aerosp. Test. Semin., 2012.
[13] M.A. Underwood, T. Keller, R. Ayres, Multi-Shaker Control: A Review of the Evolving State-of-the-Art, Sound Vib. (2017) 8–16.
[14] M.A. Underwood, New Method Determines Optimized Reference SDM for MIMO Testing, in: Proc. 32nd Aerosp. Test. Semin., 2021.
[15] M. Alvarez Blanco, K. Janssens, F. Bianciardi, Target spectrum matrix definition for multiple-input- multiple-output control strategies applied on direct-field- acoustic-excitation tests, J. Phys. Conf. Ser. 744 (2016) 012179. https://doi.org/10.1088/1742-6596/744/1/012179.
[16] F. Jacobsen, T. Roisin, The coherence of reverberant sound fields, J. Acoust. Soc. Am. 108 (2000) 204–210. https://doi.org/10.1121/1.429457.
[17] P.A. Nelson, S.J. Elliott, Active Control of Sound, 3rd ed., 2007.
[18] M. Alvarez Blanco, K. Janssens, F. Bianciardi, Experimental verification of projection algorithms and optimization routines for acoustic field uniformity enhancement in MIMO direct field acoustic control, in: Proc. ISMA, 2016.
[19] P. Larkin, Developments in Direct-Field Acoustic Testing, Sound Vib. (2014) 6–10.
[20] G. Maahs, DFAT Development and Flight Testing of Radiation Belt Storm Probe (RBSP) Satellites, in: Proc. 27th Sp. Simul. Conf., 2012.
[21] G. Maahs, DFAT Development and Flight Testing of Radiation Belt Storm Probe (RBSP) Satellites, in: Proc. 27th Aerosp. Test. Semin., 2012.
[22] U. Ingard, Notes on Acoustics, Infinity Science Press LLC, 2008.
[23] L.E. Kinsler, A.R. Frey, A.B. Coppens, J. V. Sanders, Fundamentals of Acoustics, 4th ed., Wiley, 2000.
[24] A. Cicero, J.A. Hargreaves, A Boundary Element Method (BEM) solver for low frequency room modes, in: Proc. Internoise, Glasgow, 2022.
[25] A.G. de Miguel, M. Alvarez Blanco, E. Matas, H. Beriot, J. Cuenca, I.C.S. Ngan, B. Peeters, Numerical Pre-Test Analysis for Multi-Channel Control Strategies in Environmental Acoustic Tests, in: Proc. ECSSMET, 2021.
[26] M.A. Underwood, Comparisons of the Structural Response of a Test Article Excited by DFAT™ Diffuse and Non-Diffuse Acoustic Fields, in: Proc. 91st Shock Vib. Symp., Orlando, 2021.
[27] A.J. Berkhout, D. de Vries, P. Vogel, Acoustic control by wave field synthesis, J. Acoust. Soc. Am. 93 (1993) 2764–2778. https://doi.org/10.1121/1.405852.
[28] A. Carrella, W. Mayne, Insight into the sound field during a Direct Field Acoustic Test (DFAT), in: Proc. Internoise2, Glasgow, 2022.
[29] M. Nolan, E. Fernandez-Grande, J. Brunskog, C.-H. Jeong, A wavenumber approach to quantifying the isotropy of the sound field in reverberant spaces, J. Acoust. Soc. Am. 143 (2018) 2514–2526. https://doi.org/10.1121/1.5032194.